



THE UNIVERSITY *of* EDINBURGH

Edinburgh Research Explorer

Have human activities changed the frequencies of absolute extreme temperatures in eastern China?

Citation for published version:

Wang, J, Tett, SFB, Yan, Z & Feng, J 2018, 'Have human activities changed the frequencies of absolute extreme temperatures in eastern China?', *Environmental Research Letters*, vol. 13, no. 1, 014012. <https://doi.org/10.1088/1748-9326/aa9404>, <https://doi.org/10.1088/1748-9326/aa9404>

Digital Object Identifier (DOI):

[10.1088/1748-9326/aa9404](https://doi.org/10.1088/1748-9326/aa9404)
[10.1088/1748-9326/aa9404](https://doi.org/10.1088/1748-9326/aa9404)

Link:

[Link to publication record in Edinburgh Research Explorer](#)

Document Version:

Peer reviewed version

Published In:

Environmental Research Letters

General rights

Copyright for the publications made accessible via the Edinburgh Research Explorer is retained by the author(s) and / or other copyright owners and it is a condition of accessing these publications that users recognise and abide by the legal requirements associated with these rights.

Take down policy

The University of Edinburgh has made every reasonable effort to ensure that Edinburgh Research Explorer content complies with UK legislation. If you believe that the public display of this file breaches copyright please contact openaccess@ed.ac.uk providing details, and we will remove access to the work immediately and investigate your claim.



Have human activities changed the frequencies of absolute extreme temperatures in eastern China?

Jun Wang^{1*}, Simon F B Tett², Zhongwei Yan^{1,3} and Jinming Feng¹

¹ Key Laboratory of Regional Climate-Environment for Temperate East Asia, Institute of Atmospheric Physics, Chinese Academy of Sciences, Beijing, China

² National Center for Atmospheric Sciences-Climate & School of GeoSciences, The University of Edinburgh, Edinburgh, United Kingdom

³ University of Chinese Academy of Sciences, Beijing, China

Corresponding author: Jun Wang (wangjun@tea.ac.cn)

Abstract

Extreme temperatures affected the populous regions, like eastern China, causing substantial socio-economic losses. It is beneficial to explore whether the frequencies of absolute or threshold-based extreme temperatures have been changed by human activities, such as anthropogenic emissions of greenhouse gases (GHGs). In this study, we compared observed and multi-model-simulated changes in the frequencies of summer days, tropical nights, icing days, and frost nights in eastern China for the years 1960-2012, using an optimal fingerprinting method. Observed long-term trends in the regional mean frequencies of these four indices are +2.36, +1.62, -0.94, -3.02 days decade⁻¹. Models perform better in simulating the observed frequency change in daytime extreme temperatures than nighttime ones. Anthropogenic influences are detectable in the observed frequency changes of these four temperature extreme indices. The influence of natural forcings cannot be robustly detected in any indices. Further analysis found that the effects of GHGs changed the frequencies of summer days (tropical nights, icing days, frost nights) by +3.48±1.45 (+2.99±1.35, -2.52±1.28, -4.11±1.48) days decade⁻¹. Other anthropogenic forcing agents (dominated by anthropogenic aerosols) offset the GHGs effect and changed the frequencies of these four indices by -1.53±0.78, -1.49±0.94, +1.84±1.07, +1.45±1.26 days decade⁻¹, respectively. Little influence of natural forcings was found in the observed frequency changes of these four temperature extreme indices.

1. Introduction

Extreme temperatures bring a substantial risk to human health, agriculture, and ecosystem services (Field *et al* 2012). Association between human activities and extreme temperatures are often studied, especially after many places on the globe have encountered unprecedented extreme weather, such as Europe in the summer of 2003 (Stott *et al* 2004), and eastern United States in the winter of 2014 (Trenary *et al* 2015). Extreme temperatures spread over central-eastern China in the summer of 2013 and eastern China in the winter of 2016, causing unprecedented death rolls and socio-economical losses (Sun *et al* 2014; Wang *et al* 2017; Qian *et al* 2017). Exploring the roles of external drivers in the frequency changes of extreme temperatures is urgent, in order to provide

58 reliable projections of extreme temperatures and indicative references for the adaptation and
59 mitigation of regional climate change.

60 Previous detection and attribution studies focused on the changes in annual maxima/minima of
61 daily temperatures (Christidis *et al* 2011; 2015; Wen *et al* 2013; Kim *et al* 2016; Yin *et al* 2017) and
62 percentile-based extreme temperatures (Christidis *et al* 2005; Morak *et al* 2011; 2013; Lu *et al*
63 2016), and indicated that human influence has contributed to these changes at global and regional
64 scales (Stott *et al* 2016). A pioneer study conducted by Hegerl *et al* (2004) examined whether the
65 changes in extreme temperatures are detectable in a perfect model configuration. They found that
66 the difficulty in detection of changes in extreme temperatures is no more than the detection of
67 changes in its mean state. Christidis *et al* (2005) first used the optimal fingerprinting method to
68 detect the anthropogenic influences on the changes in extreme temperatures during the second half
69 of the last century. As for China, Wen *et al* (2013) and Yin *et al* (2017) used an optimal detection
70 method to detect human influence on the changes in annual maxima and minima of daily
71 temperatures in China. They found that anthropogenic influences are detectable in the changes of
72 extreme temperatures in China. Lu *et al* (2016) conducted detection analysis on the frequencies of
73 percentile-based extreme temperatures in China during the period 1958-2002, and also found the
74 clear anthropogenic signals in the observed frequency changes in relatively warmer and colder days
75 and nights.

76 However, socio-economic stress from extreme temperatures is mostly felt through the changes in
77 absolute or threshold-based extreme high or low temperatures. We focus especially on absolute
78 extreme temperatures precisely because of their practical significance. Threshold-based extreme
79 temperatures directly contribute to increased discomfort and mortality rates, and agricultural and
80 hydrological disaster losses (Basu and Samet 2002; Bai *et al* 2014; Lesk *et al* 2016). Current
81 detection and attribution studies require signals from climate model simulations. One of the major
82 challenges faced by the attribution studies of changes in threshold-based extreme temperatures is
83 that current climate models cannot well represent the mean state of surface air temperature at
84 regional scales (Sun *et al* 2015). Simulated frequency changes in the threshold-based extreme
85 temperatures tend to be sensitive to this model potential bias. Therefore, before calculating the

86 frequency of these extreme temperatures, we need to evaluate the model performance. In addition,
87 changes in daily maximum (Tmax) and minimum (Tmin) temperatures are dominated by the
88 variations of surface solar radiation and net longwave radiation, respectively (Zhou and Wang 2016).
89 Human influence on the changes in the daytime and nighttime temperatures is unlikely to be
90 identical, as is the case for extreme temperatures.

91 In this study, we choose four indices of absolute extreme temperatures as defined by the Expert
92 Team on Climate Change Detection and Indices (ETCCDI; www.climdex.org/indices.html) and
93 previous studies (Alexander *et al* 2006; Zhang *et al* 2011) and study the frequency changes in
94 daytime and nighttime extreme temperatures separately. We measure the days with Tmax higher
95 than 25 °C as summer days and the night with Tmin higher than 20 °C as tropical nights. We also
96 count the days with Tmax and Tmin lower than 0 °C as icing days and frost nights, respectively. We
97 employ an optimal fingerprinting technique to detect and attribute the influences of human
98 activities-including greenhouse gases and other anthropogenic forcings (dominated by
99 anthropogenic aerosols), and natural external forcings (combined effect of solar radiation and
100 aerosols from volcanic eruptions) in these long-term changes.

101

102 **2. Data and Methods**

103 **2.1. Observations**

104 We use a newly homogenized daily Tmax and Tmin dataset observed at 753 Chinese
105 meteorological stations for 1960-2012 (figure S1). The temperature observations we use have been
106 quality-controlled and adjusted for most non-climatic biases due to the changes in the local
107 observing system, such as station relocation (Li and Yan 2009; Li *et al* 2016).

108 Since the horizontal resolutions of climate models are in the range of 1-3 °, we divide the mainland
109 of eastern China into 2°×2° resolution grid boxes and construct a regional gridded temperature
110 dataset using available observations within each grid box. Specifically, we first calculate the
111 climatological mean annual cycle (base period: 1960-2012) and daily temperature anomalies at each
112 station. Given that temperature is dependent of elevation, for the boxes where topography has a
113 wide range and stations are unevenly distributed, there might be certain derivation in the extreme

temperatures if the gridded temperature is developed by simple averaging of the individual station within each grid box. Hence, we need to correct the elevation-related bias in the temperature mean state within each grid box. Considering the lapse rate of near-surface air temperature is time-varying and region-dependent, use of a fixed temperature lapse rate could be problematic on the complex terrains in China. Following Li *et al* (2013), we divide the whole mainland China into 24 sub-regions (figure S1). We use the multiple linear regression method including the effects of latitude, longitude, and elevation to estimate the lapse rates of Tmax and Tmin for each sub-region and each month (figure S2). Terrain-based global 0.25 °×0.25 ° land elevation and ocean depth dataset (TBASE) (http://research.jisao.washington.edu/data_sets/elevation/) is applied to estimate the averaged elevation within each grid box (figure S3). The local elevation bias in climatological mean annual cycle of the individual station is adjusted based on the spatiotemporal-varying temperature lapse rates. The final gridded dataset is obtained by adding the station average temperature anomalies to the station average elevation-bias-corrected climatological mean annual cycle for each grid box. Furthermore, to estimate the regional averages precisely, we establish a set of areal weights of land fraction by considering their latitude-dependent feature and the influence of coast and island (figure S4).

130

131 **2.2. Model Simulations**

We use the CMIP5 simulations to estimate the responses of extreme temperatures to external forcings and the internal climate variability. Table 1 lists all the available CMIP5 models used in this study. All the experiments with specific forcings have three or more members and produce daily outputs. We first evaluate the skill of climate models with ALL forcing in simulating the climatological mean of Tmax and Tmin. As shown in figures S5 and S6, climate models tend to perform better over eastern China than western China. There are two explanations for this discrepancy: (1) the station density in western China is much lower than eastern China (figure S1); (2) the topography in western China is much more complex than eastern China, which is poorly captured in models with resolutions of around 1-3 degrees (figure S3). The gridded temperature values can be affected seriously by individual station with local effects. We focus our analysis on eastern China (east of 105 °E) also because the majority of China's people live in the eastern

143 segment of the country.

144 We calculate the time series of simulated regional mean frequency of extreme temperatures in
145 eastern China, and compared them with the observed ones (figure S7). Results illustrate a good
146 consistency between the observed and simulated frequency of summer days and tropical nights in
147 eastern China, though models tend to overestimate the frequencies of icing days and frost nights in
148 eastern China by on average 33.6% (14.1 days) and 13.8% (14.4 days), respectively. However, in
149 western China, the spread of simulated frequencies of extreme temperatures is very large (figure
150 S8). It implies that CMIP5 models can hardly capture the mean state and variability of surface air
151 temperature in western China. Based on these evaluations, we focus on eastern China in this study.

152 We use 32 simulations from 5 models driven by combined anthropogenic and natural forcing (ALL);
153 23 simulations from 5 models driven by natural forcing only (NAT) and greenhouse gas forcing
154 only (GHG) (Table 1). All simulations end in 2012. The more recent years are not included in this
155 study, as most of the model simulations required for the detection analyses are ended in 2012. It is
156 assumed that the temperature extreme responses to historical anthropogenic (ANT) and NAT
157 forcings are linearly additive and the difference between the ALL and NAT responses can be
158 estimated as ANT response. Annual anomalies, with respect to 1960-2012, are computed from the
159 resulting regional average frequency of extreme temperatures from observations and individual
160 model runs, using the same sets of space data masks and areal weights. We compute the ensemble
161 means for individual models and then average the ensemble means to give the expected
162 multi-model response to large-scale external forcings. Thus, the patterns we consider are the annual
163 anomalies of the frequency of extreme temperatures.

164

165 **2.3. Optimal Fingerprinting Method**

166 We use an optimal fingerprinting method in which observations (\mathbf{y}) are expressed as a sum of scaled
167 model-simulated fingerprint patterns (\mathbf{X}) plus internal climate variability (ϵ) as $\mathbf{y} = \mathbf{X}\boldsymbol{\beta} + \epsilon$. The
168 scaling factors $\boldsymbol{\beta}$ adjust the magnitude of the fingerprints to best match the observations. The
169 multi-model ensemble averages of forced (ALL, GHG and NAT) simulations are used to estimate
170 the fingerprints, and the pre-industrial control (CTL) simulations are used to estimate internal
171 climate variability. The regression is fitted based on the Eq. (4) in Allen and Tett (1999): $\tilde{\boldsymbol{\beta}} =$

172 $(\mathbf{X}^T \mathbf{C}_N^{-1} \mathbf{X})^{-1} \mathbf{X}^T \mathbf{C}_N^{-1} \mathbf{y}$. We compute non-overlapping three-year-mean time series of the
 173 multi-model-simulated regional mean frequency of extreme temperatures as the forced response or
 174 signal for the specific forcing (\mathbf{X}), which includes 18 data values for the period 1960-2012.
 175 Observations are processed in the same way as the simulations. Fitting and testing the regression
 176 models need two independent estimates of the inversed covariance structure of internal climate
 177 variability (\mathbf{C}_N^{-1}). We use the CTL simulations and the inter-ensemble difference from forced
 178 simulations to estimate them. Time series from CTL simulations are divided into 60
 179 non-overlapping 53-year chunks and similarly masked to be in accord with observations in space.
 180 Additional 79 non-overlapping 53-year chunks are constructed using inter-ensemble differences
 181 from forced simulations (ALL: 33; GHG: 23; NAT: 23). We separate each set of chunks from CTL
 182 simulations or forced simulations into two groups sequentially. The first group of chunks is used to
 183 pre-whitening the data and the second group is used for the uncertainty analysis on the estimation of
 184 scaling factors ($\tilde{\beta}$). Instead of decreasing the dimension via a projection on the first k leading
 185 empirical orthogonal functions, we use a regularized estimate of the covariance matrix of the
 186 internal climate variability (Ribes *et al* 2009). Regularized estimate of the covariance matrix can
 187 avoid the underestimation of the lowest eigenvalues that occurs in original covariance matrix and
 188 ensure the covariance matrix is full rank (Ribes *et al* 2013). We apply Eq. (19) provided by Allen
 189 and Tett (1999) to conduct residual consistency checks to detect model inadequacy. Result show
 190 that all the regression models can pass this test, which means that climate models are able to
 191 simulate the internal variability of the frequency of extreme temperatures in eastern China
 192 reasonably well.

193 Based on the Eq. (6) and Eq. (7) in Allen and Tett (1999), we estimate the variance-covariance
 194 matrices of the internal variability noise by using the first set of non-overlapping 53-year chunks.
 195 We obtain the 5-95% uncertainty range of scaling factors by assuming that the internal variability
 196 noise is normally-distributed. To estimate the probability distribution functions of the contributions
 197 from different forcing agents, we generate random samples of 10000,000 values from the normal
 198 distribution of estimated scaling factors and multiply the forced trends in different signals by these
 199 random numbers.

200

3. Results

3.1. Patterns and one-signal detection analysis

Figure 1 shows the spatial distributions of observed trends in the frequencies of the four extreme temperature indices. Summer days have increased significantly over the northeastern China (120-135 °E, 40-55 °N; +2.67 days decade⁻¹) and the middle and lower reaches of Yangtze River (110-125 °E, 28-32 °N; +2.99 days decade⁻¹). The occurrences of tropical nights increased mainly over the Yangtze-Huaihe River basin (115-125 °E, 28-34 °N; +2.62 days decade⁻¹) and part of southern China (105-115 °E, 18-24 °N; +3.91 days decade⁻¹). Significant declining trends in icing days (-2.24 days decade⁻¹) and frost nights (-3.35 days decade⁻¹) are found in the northwest of North China (105-115 °E, 35-42 °N). Frost nights also have decreased significantly over the northeastern China (-3.52 days decade⁻¹) and the Yangtze-Huaihe River basin (-4.22 days decade⁻¹). Figure 2 displays the time evolution of the observed and simulated frequency anomalies of the four indices in eastern China. The observed changes in extreme temperatures keep pace with the multi-model-simulated responses to ALL forcing, but not with the simulated responses to NAT forcing. We first apply the optimal fingerprinting method (Allen and Tett 1999) to scale the modeled time series of extreme temperatures in eastern China with ALL forcing to best fit the observations. As shown in figure 3, one-signal analysis suggests that climate models with ALL forcing can well reproduce the observed frequency change in summer days and icing days, and has scaling factor estimates consistent with the value one though bear certain internal variability. However, climate models tend to overestimate (underestimate) the frequency change in tropical nights (frost nights). This implies that model perform better in simulating the observed frequency change in daytime extreme temperatures than nighttime extremes. Though focusing on percentile-based extreme temperatures, Lu *et al* (2016) also found that climate models with ALL forcing do a better job in reproducing the frequency changes in daytime extreme indices than nighttime indices. It may be associated with the model's deficiency in reproducing the seasonality of warming trends in T_{min} in eastern China. Lewis and Karoly (2013) found that the T_{min} trends are noticeably subdued by the CMIP5 models, particularly in the boreal winter, when shallow boundary layer and soil freezing and thawing cycles are likely difficult to be simulated realistically. On the other hand, direct visual inspection of figure 2 illustrates that the uncertainty ranges in the

scaling factors for cold extremes are larger than warm extremes, which implies smaller variability in the frequency of simulated cold extremes than that of observed ones. Other studies also found similar result existing in the changes in the maxima and minimum of daily temperatures (Morak *et al* 2013; Wen *et al* 2013; Yin *et al* 2017). A possible cause for this is that the strong internal variability of winter extreme temperatures in eastern China was underestimated by the CMIP5 climate models (figure 2 and figure S7). Increased GHG enhances downward longwave radiation and hence increases the surface air temperature and change the frequency of temperature extremes. Meanwhile, the increased water vapor in warmer atmosphere can further increase downward longwave radiation. However, other anthropogenic forcing agents (e.g., aerosols) can decrease daytime temperature and change the frequency of daytime extremes directly by obstructing downward solar radiation and indirectly by changing the properties of clouds. Natural forcing agents, such as solar variability and volcanic eruptions, may also lead to the variations of surface air temperature and change the frequency of extreme temperatures by modulating solar radiation at the surface and the interaction between aerosols and clouds. The respective roles of anthropogenic and natural forcings in the change of extreme temperatures remain to be elucidated.

3.2. Two-signal detection analysis

To detect the effects of ANT and NAT forcings in the same framework, we conduct two-signal detection analysis. As shown in figure 4, the 5-95% uncertainty ranges of ANT scaling factors for the four indices do not include zero and the 90% confidence ellipse regions do not cover the origin of x-y coordinates. This indicates that the effect of ANT forcings can be clearly detected, and the climate responses of ANT and NAT forcings can be well separated from each other. In other words, the influence of human activities is detectable in the frequency change of these four temperature extreme indices. Except summer days, the 5-95% uncertainty ranges of NAT scaling factors for other indices all include zero, suggesting that the effects of NAT forcings on their frequency changes are undetectable.

3.3. Three-signal detection analysis

To examine the influences of individual groups of anthropogenic forcing agents, we conduct

three-signal analysis to scale the model responses of GHG, OANT (ALL minus the sum of GHG and NAT) and NAT for the optimal agreement with observed frequency changes in extreme temperatures. As shown in figure 5, results reveal that the effects of anthropogenic increase in GHGs can be clearly detected in the frequency changes of these four indices. Models appear to underestimate the effects of GHG on the changes in icing days and frost nights by a factor close to two. It is inferred that the model's deficiency in the effects of GHG on the changes in cold-season extreme temperatures is associated with an underestimation of GHG-forced temperature changes in cold season in eastern China. Morak *et al* (2013) found that the HadGEM1 model significantly underestimate the changes in extreme temperatures in winter across large parts of Asia. Chen and Frauenfeld (2014) found that the winter warming in the CMIP5 models is only about half (one fourth) of the observed warming in China for the period of 1901-1999 (1950-1999). The effects of OANT are also detectable, but with larger uncertainty. For all extremes indices, OANT effects are underestimated by the models. This may be due to the omission or simplification of the indirect effects of anthropogenic aerosols in some climate models, such as CanESM2 and IPSL-CM5A-LR (Hu *et al* 2014). Except summer days, the influence of NAT forcings on other indices cannot be detected. These analyses demonstrate that human-induced rise in greenhouse gas has imposed detectable impact on the frequency change in extreme temperatures over eastern China.

276

277 **3.4. Attribution**

Based on the estimate results of three-signal analyses, we quantify contributions to the frequency changes of extreme temperatures to individual factors through multiplying the simulated trends in GHG, OANT and NAT signals by the respective scaling factors. As shown in figure 6, we find that the observed frequency changes in extreme temperatures are the net result of the counter-acting effects from GHG and OANT forcing agents, since NAT forcing imposes little influence on these changes. Among three individual components of ALL forcings, the effects of anthropogenic emission of GHG is dominant and has changed the frequencies of summer days (tropical nights, icing days, frost nights) by the rates of $+3.48 \pm 1.45$ ($+2.99 \pm 1.35$, -2.52 ± 1.28 , -4.11 ± 1.48) days decade⁻¹. Other anthropogenic forcing agents (dominated by anthropogenic aerosols) offset the GHGs effect and changed the frequencies of these four indices by -1.53 ± 0.78 , -1.49 ± 0.94 ,

+1.84±1.07, +1.45±1.26 days decade⁻¹, respectively.

3.5. Robustness test

To further evaluate the robustness of above results, we repeat these analyses based on the five-year-mean series. As shown in figure S9, results from two-signal detection analyses are generally in line with those with three-year-mean series. The influence of human activities (ANT) can be clearly detected in the observed frequency change of the four extreme indices. However, the effects of NAT forcing can no longer be detected in the change in summer days. Three-signal detection analyses based on five-year-mean series also indicate that ANT influences (GHG and OANT) are detectable in the frequency changes of extreme temperatures (figure S10). And the influence of natural forcings cannot be robustly detected in any indices. All the detection analyses suggest that anthropogenic influences are responsible for the observed frequency changes of these four temperature extreme indices.

4. Summary

In this study, we used optimal fingerprinting method to compare the observed and multi-model-simulated frequency changes in four absolute extreme temperatures indices in eastern China for the period 1960-2012. Our detection analyses include two-signal analysis using climate responses to ANT and NAT forcings, and three-signal analysis using the signals of GHG, OANT, and NAT forcings. We found that the influences of human activities and natural external forcing can be clearly separated from each other. The anthropogenic influences on the frequency changes of extreme temperatures can be detected both in two-signal and three-signal detection analyses. The influence of natural forcings cannot be robustly detected in any indices. This indicates that only the effects of human activities can explain observed frequency changes in extreme temperatures in eastern China.

We further quantify the contributions of GHG, OANT and NAT forcings to the observed frequency trends of absolute extreme temperatures in eastern China during 1960-2012. Results show that the influences of GHG are dominant in the observed changes in extreme temperatures, and part of

316 which are offset by the effects of other anthropogenic forcing agents. The combined effects of GHG
317 and OANT forcings explain most of observed changes in the frequencies of extreme temperatures,
318 since the contributions of NAT forcing are quite small in the long-term changes of extreme
319 temperatures in eastern China.

320 It is worth pointing out some caveats of uncertainty existing in this study, which deserve future
321 consideration. One source of uncertainty is the systematic bias in the mean state of surface air
322 temperature between observations and simulations. We use elevation data and
323 spatiotemporal-varying temperature lapse rates to correct the topography-related bias in the
324 climatological mean annual cycle of each grid box. However, model simulations still have a small
325 systematic bias in the climatological annual mean temperature in eastern China (figure S5 and S6).
326 This discrepancy may partly be attributed to regional land use change, which may have substantial
327 effect on the observed change in extreme temperatures. The previous study suggested that the
328 effects of land use change were detectable from other anthropogenic forcings on a quasi-global
329 scale (Christidis *et al* 2013). For eastern China, the most typical land use change is urbanization,
330 which could change the climatology and long-term trend of near-surface air temperature. However,
331 it remains controversies about the extent to which urbanization has contributed to the observed
332 warming trends in Chinese urban stations (Wang and Yan 2016; Sun *et al* 2016; Ren *et al* 2017). A
333 recent study quantified the relationship between trends in urban fraction and local urban warming
334 rate in temperature records in China (Wang *et al* 2017). They found that regional average trend of
335 urban-related warming in eastern China is less than 10% of overall warming trend. Nevertheless, a
336 robust technique used for correcting local urban warming bias in temperature records is urgently
337 required for the detection and attribution of climate change in rapidly urbanizing regions.

338 Our conclusions based on trend attribution analyses are consistent with the case studies of event
339 attribution of recent extreme hot and cold temperatures in eastern China: anthropogenic influence
340 has caused a substantial increase (decrease) in the likelihood of extreme hot (cold) temperatures
341 (Sun *et al* 2014; Qian *et al* 2017). In this summer, many densely populated and economically
342 developed cities in eastern China were attacked by extreme hot temperatures for more than two
343 weeks. The city of Shanghai even experienced record-breaking high temperature on 21 July 2017

since the establishment of the benchmark meteorological station (Xujiahui) in 1872. The rapid development of urbanization in the region might further enhance the heatwave events in the urban areas (Wang *et al* 2017). Undoubtedly, human-induced increase in extreme hot temperatures, combined with the explosive growth in population and wealth, will cause enhanced risks for ecosystems, agriculture, energy production, and human health if timely and sufficient adaptation measures are not taken.

Acknowledgements

This study was supported by the National Key R&D Program of China (2016YFA0602501). Jun Wang was supported by the China Postdoctoral Science Foundation (119100581W). Simon F B Tett was supported by CSSP-China and NCAS-Climate (R8/H12/83/029). Zhongwei Yan acknowledges the support from the National Natural Science Foundation of China (41475078) and Jinming Feng acknowledges the support from the National Key R&D Program of China (2016YFA0600403).

References

- Alexander L V, Zhang X, Peterson T C *et al* 2006 Global observed changes in daily climate extremes of temperature and precipitation *J. Geophys. Res.* **111** D05109
- Allen M R and Tett S F B 1999 Checking for model consistency in optimal fingerprinting *Clim. Dyn.* **15** 419-434
- Bai L *et al* 2014 The effects of summer temperature and heat waves on heat-related illness in a coastal city of China, 2011-2013 *Environ. Res.* **132** 212-219
- Basu R and Samet J M 2002 Relation between elevated ambient temperature and mortality: A review of the epidemiologic evidence *Epidemiol. Rev.* **24** 190-202
- Chen L and Frauenfeld O W 2014 Surface air temperature changes over the twentieth and twenty-first centuries in China simulated by 20 CMIP5 models *J. Clim.* **27** 3920-3937

373 Christidis N, Stott P A, Brown S, Hegerl G C and Caesar J 2005 Detection of changes in
 374 temperature extremes during the second half of the 20th century *Geophys. Res. Lett.* **32**
 375 L20716

376 Christidis N, Stott P A and Brown S J 2011 The role of human activity in the recent warming of
 377 extremely warm daytime temperatures *J. Clim.* **24** 1922-1930

378 Christidis N, Stott P A, Hegerl G C and Betts R A 2013 The role of land use change in the recent
 379 warming of daily extreme temperatures *Geophys. Res. Lett.* **40** 589-594

380 Christidis N, Stott P A and Zwiers F W 2015 Fast-track attribution assessments based on
 381 pre-computed estimates of changes in the odds of warm extremes *Clim. Dyn.* **45** 1547

382 Hegerl G C, Zwiers F W, Stott P A and Kharin V V 2004 Detectability of anthropogenic changes in
 383 annual temperature and precipitation extremes *J. Clim.* **17** 3683-3700

384 Hu N, Li L and Wang B 2014 The role of the aerosol indirect effect in the Northern Indian Ocean
 385 warming simulated by CMIP5 models *Atmos Oceanic Sci. Lett.* **7** 411-416

386 Field C B *et al* 2012 Managing the risks of extreme events and disasters to advance climate change
 387 adaptation *Cambridge University Press* 592pp

388 Kim Y H *et al* 2016 Attribution of extreme temperature changes during 1951-2010 *Clim. Dyn.* **46**
 389 1769

390 Lesk C, Rowhani P and Ramankutty N 2016 Influence of extreme weather disasters on global crop
 391 production *Nature* **529** 84-87

392 Lewis S C and Karoly D J 2013 Evaluation of historical diurnal temperature range trends in CMIP5
 393 models *J. Clim.* **26** 9077-9089

394 Li X *et al* 2013 Near-surface air temperature lapse rates in the mainland China during 1962-2011 *J.*
 395 *Geophys. Res. Atmos.* **118** 7505-7515

396 Li Z and Yan Z 2009 Homogenized daily mean/maximum/minimum temperature series for China
 397 from 1960-2008 *Atmos. Oceanic Sci. Lett.* **2** 237-243

398 Li Z, Cao L, Zhu Y and Yan Z 2016 Comparison of two homogenized datasets of daily
 399 maximum/mean/minimum temperature in China during 1960-2013 *J. Meteorol. Res.* **30**

400 53-66

401 Lu C, Sun Y, Wan H, Zhang X and Yin H 2016 Anthropogenic influence on the frequency of
402 extreme temperatures in China *Geophys. Res. Lett.* **43** 6511-6518

403 Morak S, Hegerl G C and Kenyon J 2011 Detectable regional changes in the number of warm
404 nights *Geophys. Res. Lett.* **38** L17703

405 Morak S, Hegerl G C and Christidis N 2013 Detectable changes in the frequency of temperature
406 extremes *J. Clim.* **26** 1561-1574

407 Qian C, Wang J, Dong S, Yin H, Burke C, Ciavarella A, Dong B, Freychet N, Lott F C and Tett S
408 2017 Human influence on the record-breaking cold event in January of 2016 in Eastern China
409 *Bull. Amer. Meteor. Soc.* In press

410 Ren G, Ding Y and Tang G 2017 An overview of mainland China temperature change research *J.*
411 *Meteor. Res.* **31** 3-16

412 Ribes A, Aza   J-M and Planton S 2009 Adaptation of the optimal fingerprint method for climate
413 change detection using a well-conditioned covariance matrix estimate *Clim. Dyn.* **33** 707-722

414 Ribes A, Planton S and Terray L 2013 Application of regularised optimal fingerprinting to
415 attribution. Part I: method, properties and idealised analysis *Clim. Dyn.* **41** 2817–2836

416 Stott P A, Stone D A and Allen M R 2004 Human contribution to the European heatwave of 2003
417 *Nature* **432** 610-613

418 Stott P A *et al* 2016 Attribution of extreme weather and climate-related events *WIREs Clim Change*
419 **7** 23-41

420 Sun Q, Miao C and Duan Q 2015 Comparative analysis of CMIP3 and CMIP5 global climate
421 models for simulating the daily mean, maximum, and minimum temperatures and daily
422 precipitation over China *J. Geophys. Res. Atmos.* **120** 4806-4824

423 Sun Y *et al* 2014 Rapid increase in the risk of extreme summer heat in eastern China *Nature Clim.*
424 *Change* **4** 1082-1085

425 Sun Y *et al* 2016 Contribution of urbanization to warming in China *Nature Clim. Change* **6** 706-709

426 Trenary L, Delsole T, Tippett M K and Doty B 2015 Was the cold eastern US winter of 2014 due to
 427 increased variability? [in “Explaining Extremes of 2014 from a Climate Perspective”] *Bull.*
 428 *Amer. Meteor. Soc.* **96** S15-S19

429 Wang J and Yan Z 2016 Urbanization-related warming in local temperature records: A review
 430 *Atmos. Oceanic Sci. Lett.* **9** 129-138

431 Wang J, Yan Z, Quan X and Feng J 2017 Urban warming in the 2013 summer heat wave in eastern
 432 China *Clim. Dyn.* **48** 3015-3033

433 Wang J, Tett S F B and Yan Z 2017 Correcting urban bias in large-scale temperature records in
 434 China, 1980-2009 *Geophys. Res. Lett.* **44** 401-408

435 Wang S *et al* 2017 Accelerated increase in the Arctic tropospheric warming events surpassing
 436 stratospheric warming events during winter *Geophys. Res. Lett.* **44** 3806–3815

437 Wen H, Zhang X, Xu Y and Wang B 2013 Detecting human influence on extreme temperatures in
 438 China *Geophys. Res. Lett.* **40** 1171-1176

439 Yin H, Sun Y, Wan H, Zhang X and Lu C 2017 Detection of anthropogenic influence on the
 440 intensity of extreme temperatures in China *Int. J. Climatol.* **37** 1229-1237

441 Zhang X, Alexander L, Hegerl G C *et al* 2011 Indices for monitoring changes in extremes based on
 442 daily temperature and precipitation data *WIREs Clim Change* **2** 851-870

443 Zhou C and Wang K 2016 Coldest temperature extreme monotonically increased and hottest
 444 extreme oscillated over Northern Hemisphere land during last 114 years *Sci. Rep.* **6** 25721
 445
 446
 447
 448
 449
 450
 451
 452
 453
 454

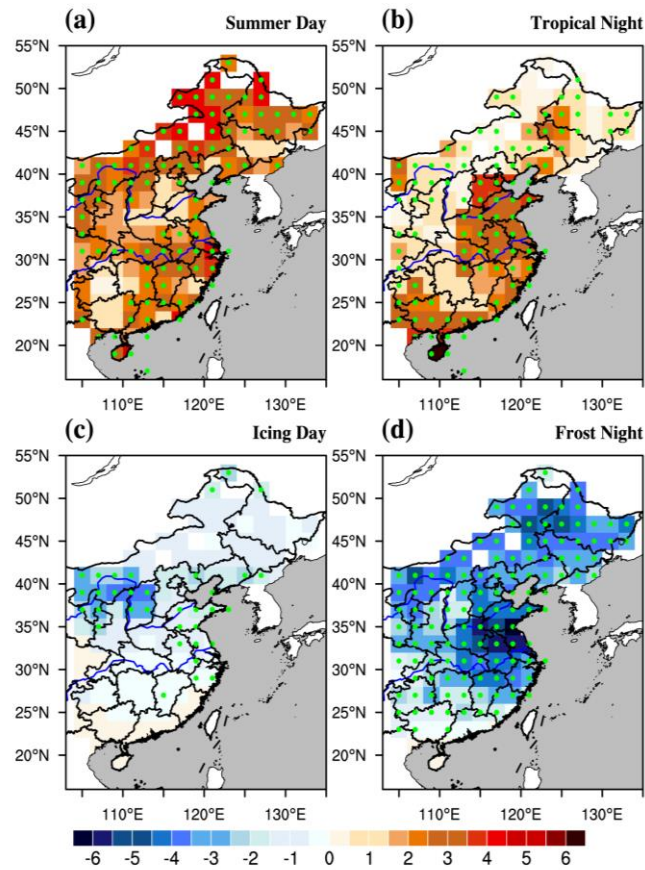


Figure 1. Observed trends (days decade⁻¹) in the frequencies of (a) summer days, (b) tropical nights, (c) icing days, and (d) frost nights in eastern China during the years of 1960-2012. Green dots represent the grid boxes where the trend is significant at the 95% confidence level. Linear trends in the frequencies of extreme temperatures were estimated by using the ordinary least squares method, with Student's *t* test for testing statistical significance.

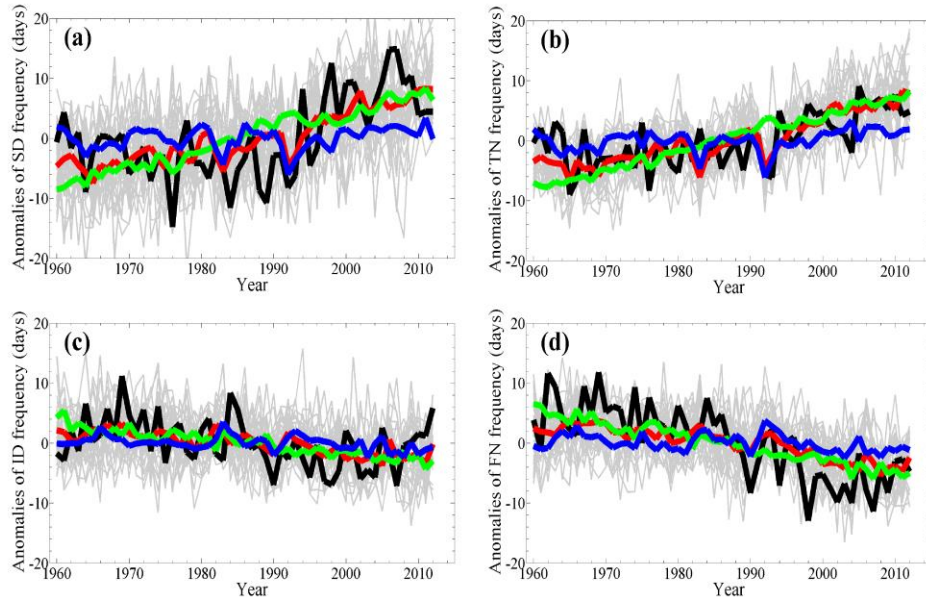


Figure 2. Observed and simulated regional averaged frequency of the four extreme temperature indices (a: summer days; b: tropic nights; c: icing days; d: frost nights) in eastern China. Annual mean anomalies in terms of the frequency of extreme temperatures are calculated with respect to its 1960-2012 mean. Solid black, red, green and blue lines represent the observations and multi-model responses to ALL, GHG and NAT forcings, respectively. Thin gray lines show the results from individual simulations of five different CMIP5 climate models.

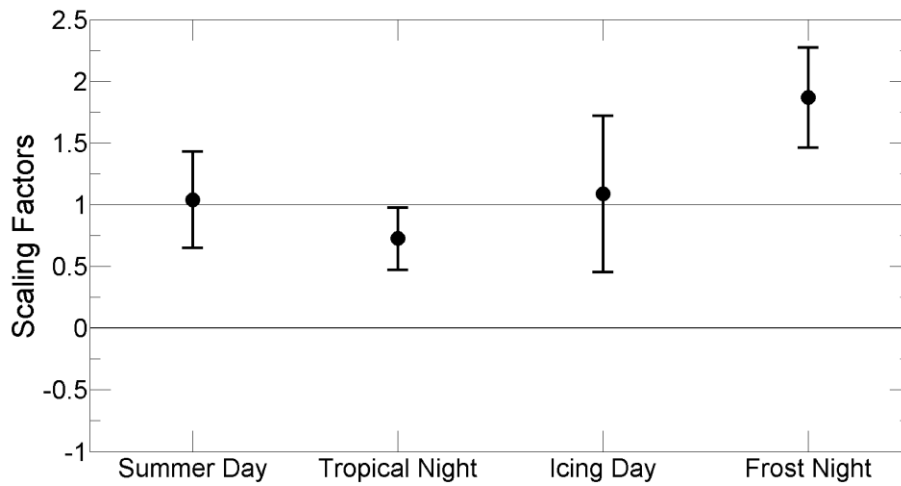


Figure 3. Scaling factors for changes in the annual frequencies of the four extreme temperature indices. Best estimates of the scaling factors that scale ALL signal patterns in one-signal detection analysis to best reproduce the observed annual anomalies of the frequency of extreme temperatures. The vertical bar marks the 5-95% uncertainty range for each signal.

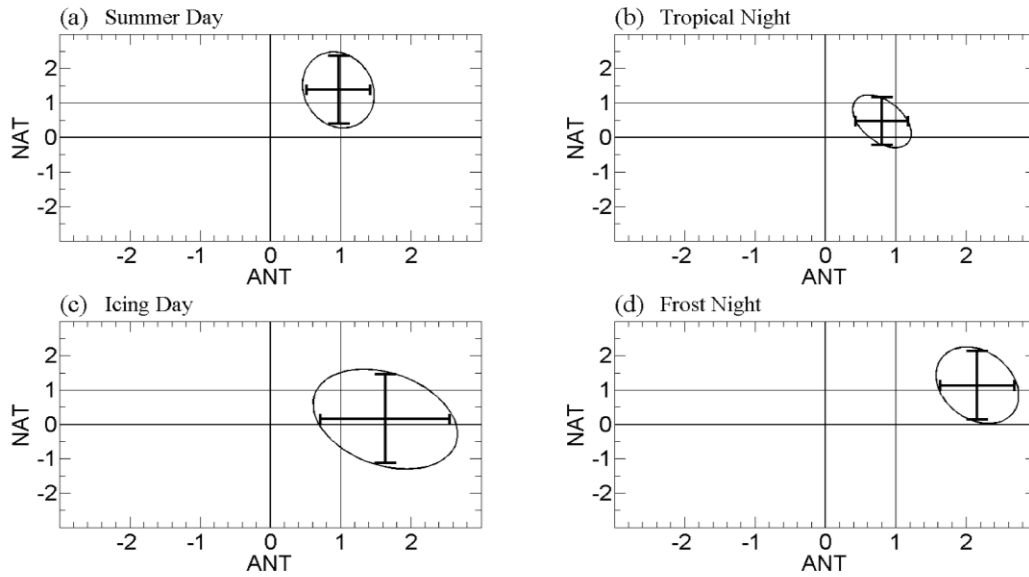


Figure 4. Scaling factors for changes in the annual frequencies of the four extreme temperature indices. Best estimates of the scaling factors that scale ANT and NAT signal patterns in two-signal detection analysis to best reproduce the observed annual anomalies of the frequency of extreme temperatures. The vertical bars mark the 5-95% uncertainty range for each signal, and the ellipses mark the two-dimensional 90% confidence region.

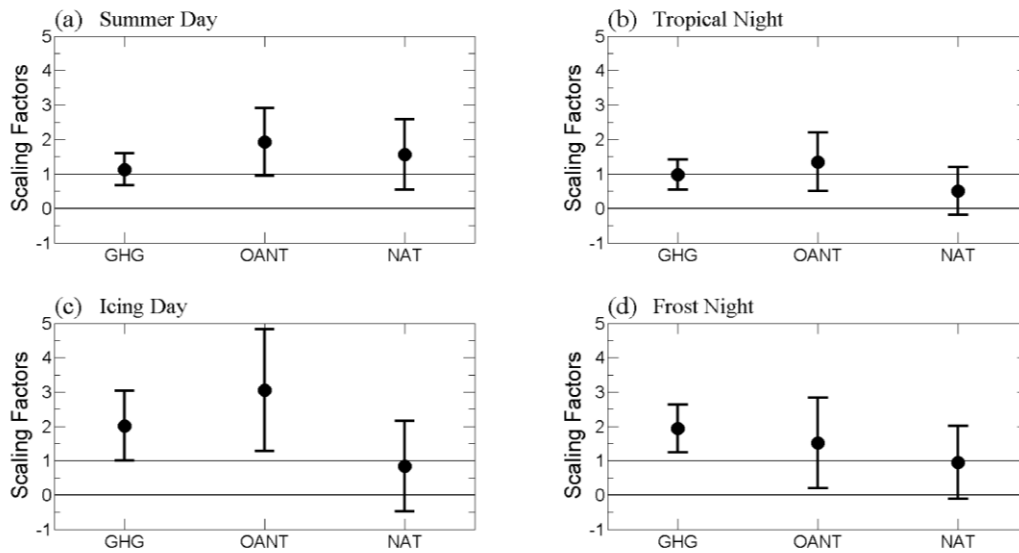


Figure 5. Scaling factors for changes in the annual frequencies of the four extreme temperature indices. Best estimates of the scaling factors that scale GHG, OANT, and NAT signal patterns in the three-signal detection analysis to best reproduce the observed annual mean anomalies of the frequency of extreme temperatures, and their 5-95% confidence intervals.

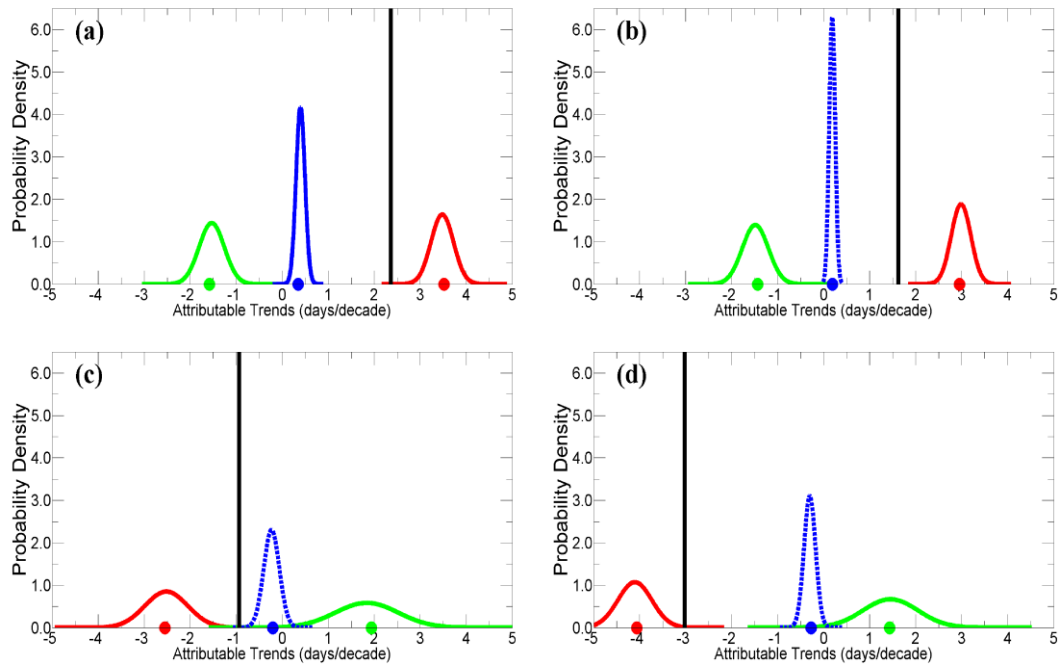


Figure 6. The attributable trends (days decade⁻¹) in the annual frequencies of the four extreme temperature indices. Best estimate of the observed trends in the frequency of extreme temperatures (bold black lines) and attributable trends due to GHG (red lines), OANT (green lines) and NAT (blue lines) from three-signal analysis. The solid (dashed) colored line indicates that the attributed frequency change is statistically significant (insignificant from zero) at a confidence level of 95%. The colored dots represent the mean attributed frequency change due to different external forcings.

541 **Table 1.** The CMIP5 models used in the optimal fingerprinting analyses. Numbers represent the
542 ensemble sizes of the ALL, NAT, GHG simulations, the years of CTL simulations, and the spatial
543 resolutions of atmospheric component of climate models. Aerosol species considered in each model
544 are also shown.

Model	ALL	NAT	GHG	CTL	Spatial resolution (lat & lon)		Aerosol species
CanESM2	5	5	5	636	2.7906°	2.8125°	SO ₄ , BC, OA, DS, SS
CNRM-CM5	10	6	6	636	1.4008°	1.4063°	SO ₄ , BC, OA, DS, SS
CSIRO-Mk3-6-0	10	5	5	424	1.8653°	1.875°	SO ₄ , BC, OA, DS, SS
HadGEM2-ES	4	4	4	530	1.25°	1.875°	SO ₄ , AN, BC, OA, DS, SS
IPSL-CM5A-LR	4	3	3	954	1.8947°	3.75°	SO ₄ , BC, OA, DS, SS
total	33	23	23	3180			

545 Notes: SO₄, sulfate; AN, ammonium nitrate; BC, black carbon; OA, organic carbon (including primary and
546 secondary organic carbon); DS, dust; SS, sea salt.